NJC

Accepted Manuscript

This is an *Accepted Manuscript*, which has been through the Royal Society of Chemistry peer review process and has been accepted for publication.

Accepted Manuscripts are published online shortly after acceptance, before technical editing, formatting and proof reading. Using this free service, authors can make their results available to the community, in citable form, before we publish the edited article. We will replace this *Accepted Manuscript* with the edited and formatted *Advance Article* as soon as it is available.

You can find more information about *Accepted Manuscripts* in the Information for Authors.

Please note that technical editing may introduce minor changes to the text and/or graphics, which may alter content. The journal's standard Terms & Conditions and the Ethical guidelines still apply. In no event shall the Royal Society of Chemistry be held responsible for any errors or omissions in this *Accepted Manuscript* or any consequences arising from the use of any information it contains.

ROYAL SOCIETY OF CHEMISTRY

www.rsc.org/njc

Structural, spectroscopic, magnetic behavior and DFT investigations of L-tyrosinato nickel(II) coordination polymer

Agnieszka Wojciechowska, [*a] *, Jan Janczak,* [b] *Zbigniew Staszak,*[c] *Marek Duczmal,*[a] *Wiktor Zierkiewicz,* [a] *Jadwiga Tokar* [a] *and Andrew Ozarowski* [d]

[a] Faculty of Chemistry, Wroclaw University of Technology, Wybrzeże Wyspiańskiego 27, 50-370 Wroclaw, Poland, Phone: +48 713203666; Fax: +48 71 320 43 60

[b] Institute of Low Temperature and Structure Research Polish Academy of Sciences, Okólna 2, 50-422 Wroclaw

[c] Faculty of Computer Science and Management, Wroclaw University of Technology, Wybrzeże Wyspiańskiego 27, 50-370 Wroclaw

[d] National High Magnetic Field Laboratory, Florida State University, 1800 East Paul Dirac Drive, Tallahassee, Florida 32310

Corresponding Author. Agnieszka Wojciechowska, Faculty of Chemistry, Wroclaw University of Technology, Wybrzeże Wyspiańskiego 27, 50-370 Wroclaw, Poland, Phone: +48 713203666; Fax: +48 71 320 43 60.

KEYWORDS *L-tyrosine, nickel(II) complex, crystal structure, spectroscopy (FT-IR, FT-Raman, NIR-vis-UV), high-field EPR, magnetic properties, DFT calculations,*

New 1D-coordination polymer {[Ni(L-Tyr)$_2$(μ-4,4'-bpy)]·4H$_2$O}$_n$ (**1**) (L-Tyr = L-tyrosine, 4,4'-bpy = 4,4'-bipyridne) composes L-tyrosinate anions chelated the nickel(II) centres via N amino and O carboxylate atoms, whereas the apices of the elongated octahedral coordination sphere are occupied by the N atoms of the 4,4'-bipyridine. Its molecular structure was determined by single-crystal X-ray diffraction and characterized by using vibrational (FT-IR), Raman (FT-Raman), electronic (NIR-Vis-UV) and high field electron paramagnetic resonance (HF-EPR) spectroscopy and thermal (TG-DTA, DSC) and magnetic methods. The tetragonality distortion parameter (T) equals to 0.945. The g_x, g_y and g_z parameters (HF-EPR spectra) are slightly temperature dependent and the set g_x = 2.178(5), g_y = 2.156(4), g_z = 2.19(1), D = -5.76(2) cm^{-1}, E = -0.41(1) cm^{-1} was found at 5 K. The analysis of the temperature and field dependent magnetization shows the weakness of magnetic interactions in **1**.

1.INTRODUCTION

L-tyrosine (L-2-Amino-3-(4-hydroxyphenyl)propanoic acid) is prepared from the phenylalanine [1-5a], it forms in hydroxylation by the Fenton reaction [5b] and is also produced by *E. coli* bacteria or higher plants. [6-9] L-tyrosine takes part in the dopamine metabolism,[10] which in turn can be converted into the catecholaminate neurotransmitters: norepinephrine and epinephrine.[11] It is recommended to be applied for enhancing memory and boosting the immune system thus it is generally considered as a safe diet in nemaline myopathy,[12] in the treatment of maternal phenyloketonuria[13], it is suggested as an antidepressant[14-15] and used as a great 'anti-stress' supplement.[16] Also, it is a precursor of human skin pigment – melanin [17] and as a hormone-like regulator of melanocytes function. [18] But, the most important is the role of a precursor of two

hormones of thyroid, triiodothyronine (T3) and thyroxine (T4). Both hormones are involved in the metal-induced fat thermogenesis process. [19-20] If the conversion of L-phenylalanine to L-tyrosine with the participation of hydrolase is unsettled, the concentration of L-Tyr is insufficient to the commencement of tyroxine synthesis.[21-23]

L-tyrosine is widely applied in many fields.[24-27] This amino acid and its derivatives, their polymeric forms, as well as metal ions complexes have been used as ecofriendly catalysts, [25] components of biomaterials [26] or as a tracer in positron emission tomography (PET).[27-28]

Studies of L-tyrosinate anion interaction with metal ions lead to the understanding of the complex formation and the stability of its complexes in the solid state and, also, in solvents. The formation of complexes is controlled by solution acidities, which is related with the p*Ka* values (2.2 for COOH and 9.1 for NH_3^+ groups). The most typical coordination mode of L-tyrosine is its chelating via N amino and one of O atoms of carboxylate groups [29-34], what is accompanied by the μ-bridging mode of carboxylate group. [35-37]. The diversity of the binding modes of the COO^- group generates monomeric, dimeric and metal-organic frameworks (MOFs). Interestingly, phenolate oxygen atoms have also been engaged in coordination to the metals ions by applying synthesis under solvothermal conditions with pH 9-10 range for deprotonation of the phenoxy group. [35b, 38]

The biological synthesis pathways of neurotransmitters, hormone of thyroid and melanin are strongly dependent on the L-tyrosine concentration in blood. The ability to form the metal-organic complexes [39-44] could decrease its concentration in fluids. The complex formation begins on the amino acid side-chain, then the HA^- anions containing the protonated phenolic

hydroxyl group is formed. [39, 40] The HA^- anions bind nickel(II) ions and form complexes of the type : $[MHA]^+$, $[MH_2A_2]$ and $[MH_3A_3]^-$ but the $[NiH_2A_2]$ units are most favorable.[29, 34c, 44b, 45]

To understand coordination properties of L-tyrosinate anions, we synthesized a novel and rare L-tyrosinato nickel(II) complex of formula $\{[Ni(L\text{-}Tyr)_2(\mu\text{-}4,4'\text{-}bpy)]\cdot 4H_2O\}_n$ (**1**). In this work, we examined the X-ray structure and spectroscopic (FT-IR, FT-Raman, NIR-vis-UV and HF-EPR) properties. The analysis of crystal structure is combined with thermal analysis and density functional theory (DFT) calculations, whereas high-frequency electron paramagnetic resonance is supported by the magnetic characterization.

2. EXPERIMENTAL SECTION

Materials $NiCl_2\cdot 6H_2O$, L-tyrosine disodium salt, 4,4'-bpy hydrate, ethanol were obtained from Sigma-Aldrich and were used without further purification.

Theoretical studies and physical measurements. Full geometry optimizations were performed by means of the three-parameter hybrid B3LYP density functional method [49-50] combined with the D95V(d, p) [51] basis set for all ligand atoms. For the Ni atom the LanL2DZ [52] effective core potential with the concomitant valence basis set was applied. BSSE (Basis Set Superposition Error) corrections of the interaction energies were performed by the counterpoise method. [53]All computations were carried out with Gaussian 09 set of programs.[54] ATR–FTIR spectra were obtained using a Brucker Vertex 70 v Fourier transform infrared spectrometer equipped with a diamond ATR cell. The FT-Raman spectra were collected on a Bruker MultiRam spectrometer (Nd:YAG laser with emitting radiation at a wavelength of 1064 nm equipped. The Raman spectrum of **1** was measurement using a wavelength 532 nm and power 2 mW. The electronic diffuse-reflectance and absorption in DMSO spectra were collected on the Cary 500 Scan UV-

Vis-NIR spectrophotometer. The absorption spectra were recorded for concentration of 1.13 × 10^{-2} M (**1**) and 2.26 ×10^{-3} M (L-Tyr). In order to obtain the bands positions, the variable digital filtering analysis was applied. [55-56] High-field, high-frequency EPR spectra at temperatures ranging from *ca.* 5 K to 30 K were recorded on a home-built spectrometer at the EMR facility of the NHMFL.[57] The microwaves were generated by a phase-locked Virginia Diodes source generating frequency of 13 ± 1 GHz and producing its harmonics of which the 2^{nd}, 4^{th}, 6^{th}, 8^{th}, 16^{th}, 24^{th} and 32^{nd} were available resulting in the frequency range ~24 to 448 GHz. A superconducting magnet (Oxford Instruments) capable of reaching a field of 17 T was employed. The magnetic susceptibility of complex **1** in the temperature range from 1.79 to 300 K in a field of 500 mT and magnetization up to 5 T were measured with a Quantum Design SQUID magnetometer. The diamagnetic correction (−361×10^{-6} emu mol^{-1}) was calculated using Pascal's constants. TG-DTA analysis was carried out using a Setaram SETSYS 16/18 system. Differential scanning calorimetry (DSC) examinations were performed on a Setaram DSC 92 instrument.

X-ray Crystallography. Single crystal was used for data collection on a four-circle KUMA KM4 diffractometer equipped with two-dimensional CCD area detector. The graphite monochromatized Mo*K*α radiation (λ=0.71073 Å) and the ω-scan technique (Δω=1º) were used for data collection. Data collection and reduction, along with absorption correction, were performed using *CrysAlis* software package [46]. The structure was solved by direct methods using *SHELXS-97* [47] revealing the positions of almost all non-hydrogen atoms. The remaining atoms were located from subsequent difference Fourier syntheses. The structure was refined using *SHELXL-97* [47] with the anisotropic thermal displacement parameters. The hydrogen atoms of

the aromatic ring were constrained with C–H = 0.82 Å and $U_{iso}(H) = 1.2U_{eq}(C)$, the H atoms of CH_2 and CH groups were constrained with C–H = 0.97 Å and $U_{iso}(H) = 1.5U_{eq}(C)$, the hydrogen atoms of water molecules were constrained with O–H = 0.82(2) Å and $U_{iso}(H) = 1.5U_{eq}(O)$ and H atoms of NH_2 groups were constrained with N–H = 0.90(1) Å and $U_{iso}(H) = 1.5U_{eq}(N)$. Visualization of the structures was made with the Diamond 3.0 program. [48] This materials is available free of charge from Cambridge Crystallographic Data Centre and are available at www.ccdc.cam.ac.uk/data_request/cif under CCDC 1043354. The experimental powder XRD pattern was acquired on a PANalytical X'Pert diffractometer equipped with a Cu Ka radiation source (λ = 1.54182 °A), and operated at 40 kV and 30 mA. The data were collected at room temperature in the range of $2\theta = 5 \div 45^{o}$ (Fig. S1). The corresponding simulated powder XRD patterns were generated using Diamond 3.1 software.

Synthesis of Complex. 0.1 M aqueous solution of disodium salt of L-tyrosine (1 mmol) was mixed with 0.1 M aqueous solution of $NiCl_2$ (0.5 mmol) with continuous stirring. 0.1 M ethanolic solution of 4,4'-bpy (0.5 mmol) was added to the obtained mixture after 5 minutes. The solution was left to slowly evaporate at room temperature. The grey crystals of (**1**) were formed after 5 days. The crystals were filtered and washed with water and dried in vacuum.

Characterization data. Yield 65%, IR Raman (cm^{-1}) 1589(s), 1591(s), 1491(s), 3088, 3062, 3015, 3062, 2963, 2923, 2897, 1519. Calcd. for chemical formula $C_{28}H_{28}N_4NiO_6 \cdot 4H_2O$ (%) : elemental analysis : C, 51.95; H, 5.61; N, 8.66. Found: C, 51.93; H, 5.08; N, 8.62 %.

3. RESULTS AND DISCUSSION

X-ray Crystallography. The complex is built up of the [Ni(L-tyr)$_2$(μ-4,4'-bpy)] units and four molecules of water per one complex unit. Two L-tyrosinate anions chelate the nickel(II) ions in

trans- fashion via pairs of N11, O11 and N21, O21 atoms with 2.064 Å, 2.044 Å, 2.067 Å, 2.041 Å distances (Table 1, Fig 1).

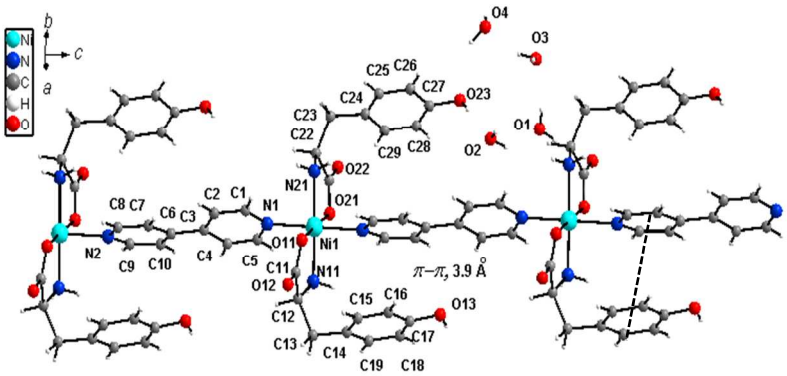

Fig. 1 The distorted octahedral environment around Ni^{2+} ions in 1D polymer chain .

Table 1 Selected Bonds (Å) Distances and Angels (deg) in **1**

Ni1—O11	2.044(4)	Ni1—N21	2.067(6)
Ni1—O21	2.041(5)	Ni1—N1	2.161(4)
Ni1—N11	2.064(6)	Ni1—$N2^{i}$	2.183(4)
N1—Ni1—$N2^{i}$	178.9(2)	O21—Ni1—N21	81.6(2)
O11—Ni1—O21	176.8(2)	O21—Ni1—N11	98.8(2)
N11—Ni1—N21	178.6(2)	O11—Ni1—N21	98.18(2)
N1—Ni—O11	91.4(2)	$N2^{i}$ —Ni1—O11	89.62(2)
N1—Ni1—N11	90.07(2)	$N2^{i}$ —Ni1—N11	89.8(2)
N1—Ni1—O21	91.79(2)	$N2^{i}$ —Ni1—O21	87.19(2)
N1—Ni1—N21	88.6(2)	$N2^{i}$ —Ni1—N21	91.5(2)
O11—Ni1—N11	81.5(2)		

Symmetry code: (*i*) *x*, *y*, *z*+1.

The apical position of the Ni^{2+} are occupied by heterocyclic 4,4'-bpy *trans*- coordinated N1 and $N2^{i}$ atoms at distances of 2.161 Å and 2.183 Å, respectively, and are close to those found for zinc(II) or iron(III) structures.[58] The coordinated N11, O11, N21, O21, N1 and $N2^{i}$ atoms create tetragonally elongated octahedral environment around Ni(II) ions. The tetragonality parameter

T equals 0.945 (T parameter is calculated as $T = R_{int} / R_{out}$, where R_{int} is the average in-plane distance and R_{out} is average out-of-plane axial distance [59]). For **1**, the tetragonal distortion of the octahedral geometry is the largest among all nickel(II) L-tyrosinato structures 2{[Ni(L-Tyr)$_2$(bpy)]}·3H$_2$O·CH$_3$OH (T = 0,996) [31], [Ni(Im)$_2$(L-Tyr)]·4H$_2$O (T = 0.995), [30] [Ni(L-Tyr)$_2$(H$_2$O)$_2$]·H$_2$O (T = 0.985) [29] investigated earlier. The chelated L-tyrosinate anions result in a slight equatorial plane deformation with the O21–Ni1–N21 and O11–Ni1–N11 angels equal 81.6 deg and 81.5 deg. The L-tyrosine entities arched their ring residues in a characteristic fashion along C12—C13—C14 and C22—C23—C24 by 112.5 deg and 117.0 deg, respectively. The L-tyr anions and 4,4'-bpy aromatic rings are parallel. Thus, the very weak intramolecular π-π interactions between them with π···π distance of ~3.9 Å are found. The distance ~3.9 Å is higher than the sum of the C-atom van der Waals radii (3.650 Å). In **1**, as in similar structures, [34k, 60-61] the N1 and N2 atoms of 4,4'-bpy join together [Ni(L-Tyr)$_2$(μ-4,4'-bpy)] complex units. The combined [Ni(L-Tyr)$_2$(μ-4,4'-bpy)] entities form 1-D polymeric chains with the neighboring nickel(II) ions distanced at 11.452 Å (Fig. 1) but the shortest possible Ni···Ni distances equal 8.557 Å and 9.494 Å, respectively.

The atoms of four molecules of water engage the carboxylate O11, O12, O22 and phenolate O13, O23 atoms as well as N11 and N21 atoms. The O23 and O22 atoms are engaged in relatively strong hydrogen bonds with O2 and O1 atoms of the water molecules, O23—H23···O2 2.644(6) Å and O1—H1*W*···O22^{iv} 2.766(5) Å (Table 2). The N11—H11*A* and N21—H21*B* atoms create hydrogen bonds with O1^{i} and O4^{iii} atoms of water molecules with D···A distances 3.003(6) Å and 3.197 (8) Å, respectively.

Table 2 Hydrogen Bonds (Å, ^{o}) stabilization the crystals of **1**

D—H···*A*	*D*—H	H···*A*	*D*···*A*	*D*—H···*A*

O13—H13···O22^{i}	0.82(1)	1.89(3)	2.633(6)	150(6)
O23—H23···O2	0.82(1)	1.86(3)	2.644(6)	160(8)
O2—H4*W*···O1	0.82(1)	2.11(4)	2.760(7)	137(6)
O1—H1*W*···O22^{iv}	0.82(1)	1.96(2)	2.766(5)	167(5)
O1—H2*W*···O3	0.82(1)	1.98(2)	2.771(7)	162(5)
O3—H5*W*···O4	0.82(1)	1.99(2)	2.774(7)	162(5)
O4—H7*W*···O13^{vi}	0.82(1)	2.01(3)	2.795(7)	161(8)
O2—H3*W*···O12^{v}	0.82(1)	2.00(1)	2.817(7)	176(9)
O3—H6*W*···O11^{v}	0.82(1)	2.09(3)	2.842(6)	153(5)
O4—H8*W*···O23	0.82(1)	2.22(5)	2.919(8)	143(8)
N11—H11*A*···O1^{i}	0.90(1)	2.12(2)	3.003(6)	166(5)
N21—H21*B*···O4^{iii}	0.90(1)	2.47(4)	3.197(8)	138(4)
N21—H21*A*···O12^{ii}	0.90(1)	2.65(5)	3.211(7)	122(4)

Symmetry codes: (i) $-x+1, y-1/2, -z+1$; (ii) $-x, y+1/2, -z$; (iii) $-x, y-1/2, -z+1$; (iv) $x, y, z+1$; (v) $-x, y+1/2, -z+1$; (vi) $x, y+1, z$;

In particular, the intermolecular interactions between the O4 atom of water molecule and phenolato O13 and O23 atoms create the O4—H7*W*···O13^{vi} and O4—H8*W*···O23 hydrogen bonds in which D···A separation equal 2.795(7) Å and 2.919(8) Å, respectively. The combination of these bonds forms the short hydrogen bond chain, which joins the parallel 1-D polymer chains (Fig. S2). Additionally, they are part of a hydrogen five membered ring together with hydrogen bonds created between the water molecules O2—H4*W*···O1, O1—H2*W*···O3 and O3—H5*W*···O4, in which the *D*···*A* distances close to 2.760-2.774 range Å. It seems that oxygen atoms of water molecules, which act both as acceptors and as donors, play an important role in crystal stabilization of **1** because only two hydrogen interactions do not contain oxygen of

water molecules. That is, the O13—H13 and N21—H21*A* groups form hydrogen bonds with uncoordinated $O22^{i}$ and $O12^{ii}$ atoms of carboxylate group with D···A distances 2.633(6) and 3.211(7) Å, respectively. These N21—H21*A*···$O12^{ii}$ hydrogen bonds connect the [Ni(L-tyr)$_2$] complex units in a zig-zag chain extended parallel to the *b* axis (Fig. 2).

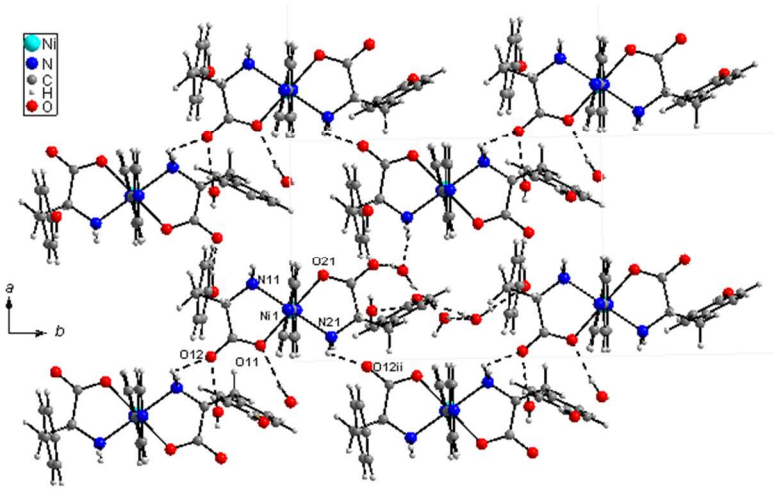

Fig. 2 The perspective view of zig-zag motive based on N21—H21A···$O12^{ii}$ bond.

Spectroscopic, Magnetic and Thermal Studies. Two asymmetric bands with maxima at *ca.* 11000 cm^{-1} and 18000 cm^{-1} are generated by the first and second of three characteristic spin-allowed transition of the Ni(II) ions and are assigned as $^3A_{2g}(F) \rightarrow {}^3T_{2g}(F)$ and $^3A_{2g}(F) \rightarrow {}^3T_{1g}(F)$ (O_h symmetry) (Fig. 3). At the right part of the first *d-d* band (*ca.* 13000 cm^{-1}) the sharp component is usually assigned to the spin-forbidden transition $^3A_{2g}(F) \rightarrow {}^1E_g(D)$. The expected third *d-d* band, assigned to the $^3A_{2g}(F) \rightarrow {}^3T_{1g}(P)$, is located in the less well shaped region of 22000-35000 cm^{-1}. The donor atoms form a *trans*-[$NiN_2N_2'O_2$] pseudo octahedral chromophore. The relatively long distances of Ni–N1 and N2 atoms of *ca.* 2.170 Å in comparison to other

atoms result in the value of T = 0.945. Such elongation in the Ni–N1 and Ni–N2^{i} bonds requires using the D_{4h} symmetry in the interpretation of the electronic spectra. In the crystal filed of elongated octahedral geometry (D_{4h}, ground state $^{3}B_{1g}$) the $^{3}T_{2g}$(F) and $^{3}T_{1g}$(F) states are split into pairs of levels $^{3}E_{g}$ + $^{3}B_{2g}$ and $^{3}A_{2g}$ + $^{3}E_{g}$, respectively.

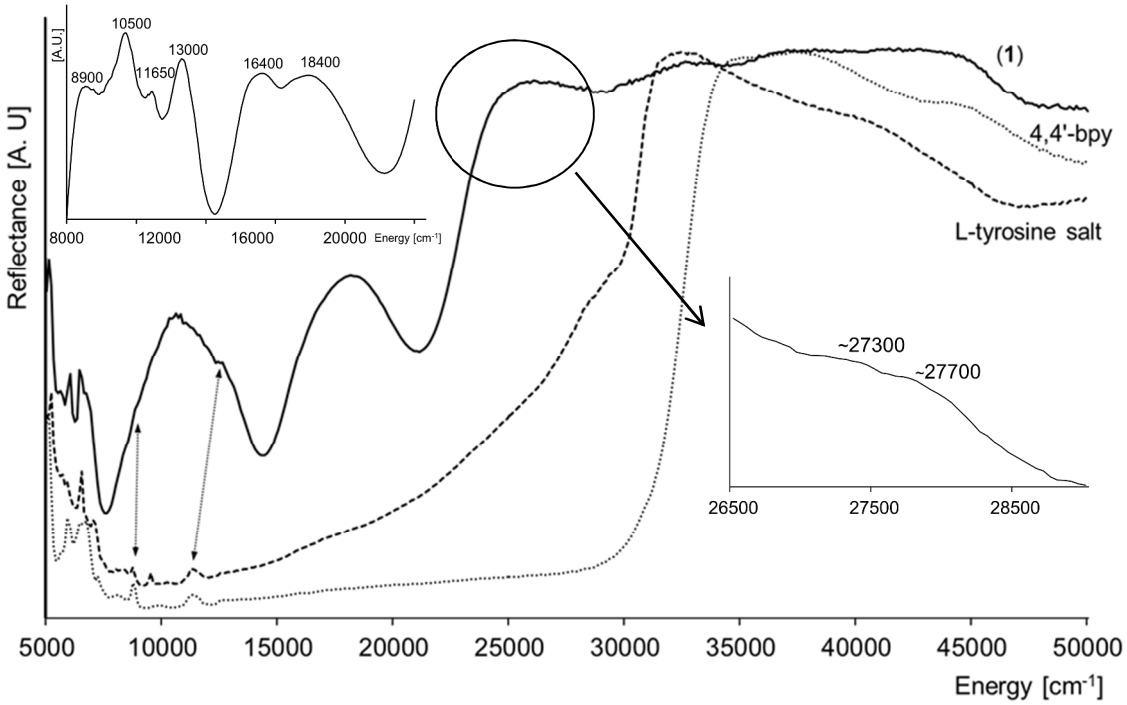

Fig. 3 Diffuse-reflectance spectrum of powdered complex **1** and ligands. In the inset : the filtration effect with parameters: step = 50, α = 200 and N = 15.

To obtain the expected components of the *d-d* bands, the spectrum was filtered (Fig. 3). The first *d-d* band splits into four components with positions at 8900, 10500, 11650, 13000 cm^{-1}, whereas the second one consists of two components at 16400 and 18400 cm^{-1}.

The first component at 8900 cm^{-1} originates from L-tyr, while the last component centered at 13000 cm^{-1} can be assigned to the pairs of spin-forbidden transitions $^{3}B_{1g} \rightarrow {}^{1}A_{1g}$ and $^{3}B_{1g} \rightarrow {}^{1}B_{1g}$ derived from the splitting of the $^{1}E_{g}$ (O_h) level. The maxima at 10500, 11650 cm^{-1} and 16400, 18400 cm^{-1} are assigned to the pairs of spin-allowed $^{3}B_{1g} \rightarrow {}^{3}E_{g}$, $^{3}B_{1g} \rightarrow {}^{3}B_{2g}$ and $^{3}B_{1g}$

$\rightarrow {}^3A_{2g}$, ${}^3B_{1g} \rightarrow {}^3E_g$ transitions, respectively. Fortunately, the detailed filtration analysis of this region revealed two extra bands at 27300 and 27700 cm^{-1} which can be assigned to the ${}^3A_{2g}$ and ${}^3E_g$ components of the third *d-d* band. Finally, from the energies 10500, 11650, 13000, 16400, 18400, 27300, 27700 cm^{-1} the crystal field parameters and Racah B were calculated: Dq = 1170 cm^{-1}, Ds = 457 cm^{-1}, Dt = 130 cm^{-1}, B = 820 cm^{-1}. These parameters are very similar to those found for $[Ni(Im)_2(L\text{-}tyr)_2]\cdot 4H_2O$ (Dq = 1180 cm^{-1}, Ds = 434 cm^{-1}, Dt = 132 cm^{-1}, B = 865 cm^{-1}) [30]. The only significant difference is in the Racah B parameter. This is probably due to the *cis*-arrangement of the imidazole nitrogen atoms in the chromophore $[NiN_2N_2'O_2]$ in the case of $[Ni(Im)_2(L\text{-}Tyr)_2]\cdot 4H_2O$ structure in contrast to *trans*- fashion for **1**.

The HFEPR spectra were interpreted by using the standard spin Hamiltonian for S = 1 :$\hat{\boldsymbol{H}} = \beta_B \boldsymbol{B}\cdot\hat{\boldsymbol{g}}\cdot\hat{\boldsymbol{S}} + D[\hat{\boldsymbol{S}}_z^2 - 1/3\cdot S(S+1)] + E(\hat{\boldsymbol{S}}_x^2 - \hat{\boldsymbol{S}}_y^2)$. (1)

The spin Hamiltonian parameters determined from spectra taken at 30 K are g_x = 2.162(3), g_y = 2.157(3), g_z = 2.190(5), D = -5.74(2) cm^{-1}, E = -0.429(7) cm^{-1}. The parameters changed slightly at 5 K: g_x = 2.178(5), g_y = 2.156(4), g_z = 2.19(1), D = -5.76(2) cm^{-1}, E = -0.41(1) cm^{-1}. The parameters were found by fitting the resonance positions in spectra measured over a frequency range ca 100 - 420 GHz (Figs. 4 and 5). In the spin triplet state, two 'allowed' ΔM_S=1 resonances are expected at each orientation of a molecule versus the magnetic field.

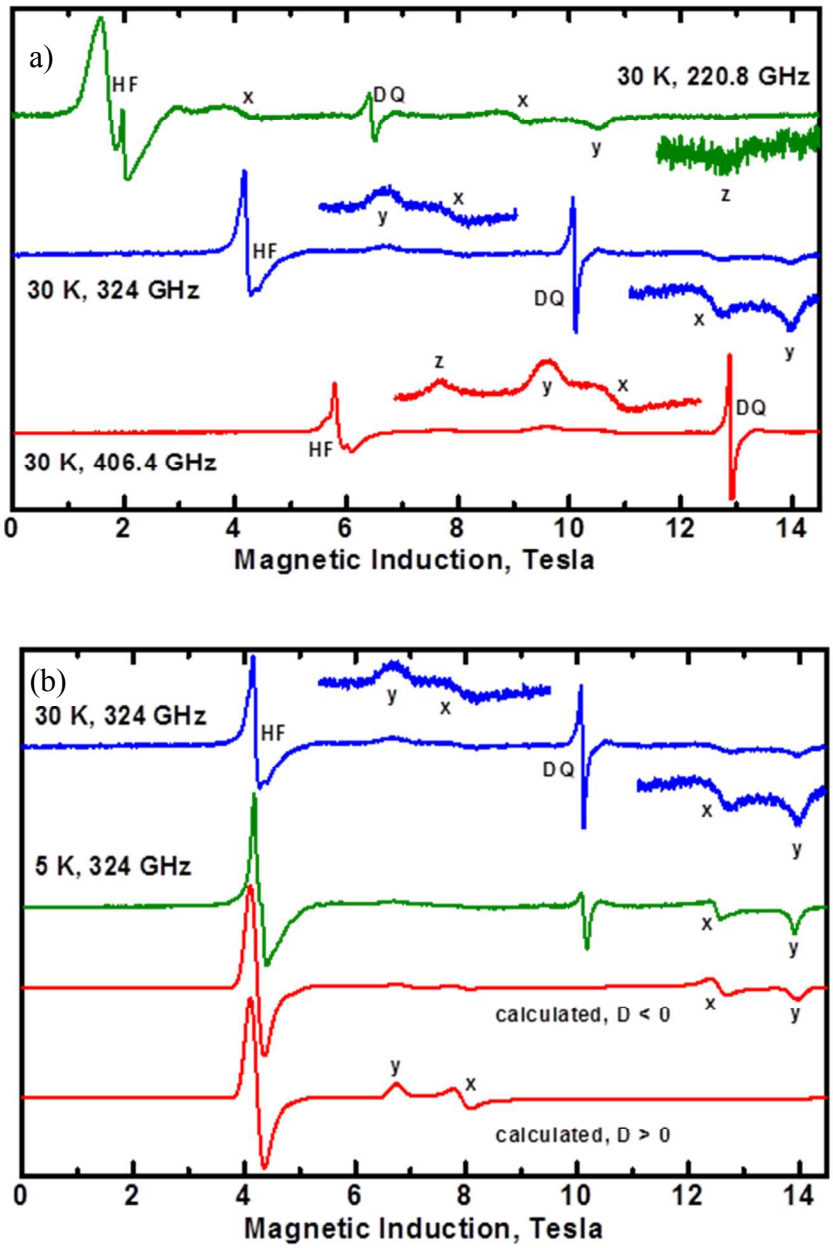

Fig. 4 (a) The EPR spectra at 30 K in 220.8, 324 and 406.4 GHz (b) 324 GHz EPR spectra recorded at temperatures indicated. The molecular orientations for respective transitions are marked with X, Y and Z.

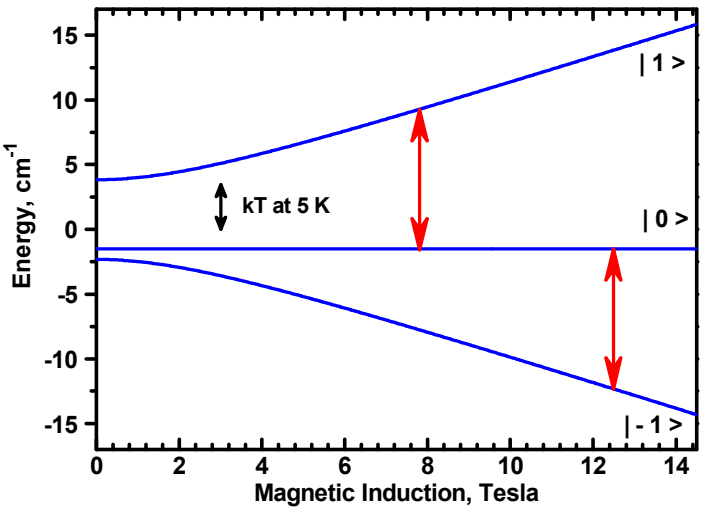

Fig. 5 Energy of the spin states in magnetic field at the "X" orientation, calculated with the spin Hamiltonian parameters of **1** (negative D and E). Red arrows represent the microwave quantum energy of 10.8 cm^{-1} (324 GHz). kT at 5 K equals 3.475 cm^{-1}. The transition occurring at the higher magnetic field starts from the lowest energy state, while the transition at lower field starts from a thermally depopulated state and will be frozen out. With a positive D, these relations would be inverted. Negative D is normally associated with $g_z > g_{x,y}$ and the parameters found here obey the relationship $D = \lambda (g_z - g_{x,y}) / 2$. [63] Taking λ = -315 cm^{-1}, [63] and the average of g_x, g_y of 2.16, we get D = -5.16 cm^{-1}, in a reasonable agreement with

In the high - frequency EPR, the microwave quantum energy is comparable to or even larger than kT at low temperatures and depending on the sign of D, one of the resonances in such a pair will be frozen out at sufficiently low temperature. The intensity ratio of the stronger resonance to the weaker in a pair is approximately equal to $R = (e^{h\nu/kT}-1)/(1-e^{-h\nu/kT})$, [62] which

evaluates to 22.4 for T = 5 K and = 324 GHz. In the X-Band EPR (9.6 GHz) that ratio is 1.09 at 5K and obviously the intensity pattern would be affected very little.

The magnetic susceptibility of **1** shows the Curie–Weiss behavior in the temperature range *ca*. 30–300 K with a Weiss constant Θ = –1.1 K and a magnetic moment of 3.06 μ_B (Figs. 6 - 7).

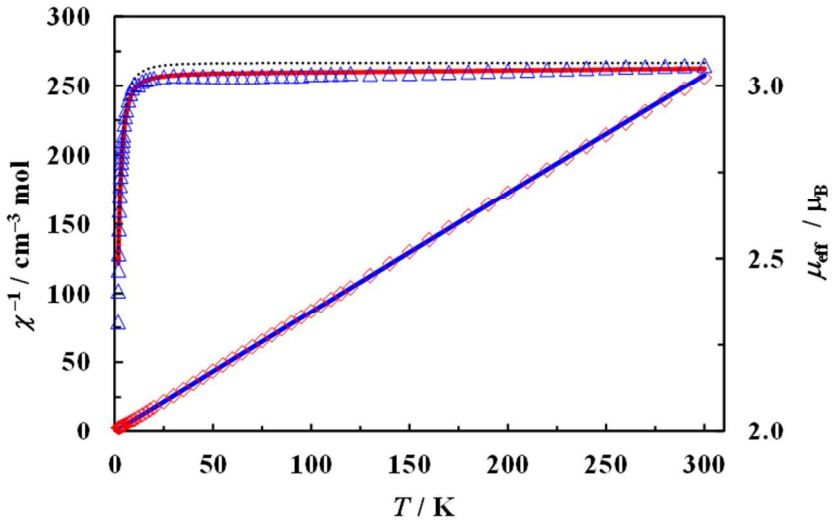

Fig. 6. Plots of χ^{-1} (◇) and μ_{eff} (Δ) versus *T* for **1**. The solid lines is the best fit parameters (*D*, *E* from HF-EPR, *g* = 0.989 g_{EPR}, *N* = 41·10^{-6}), the dotted line – all parameters from HF-EPR.

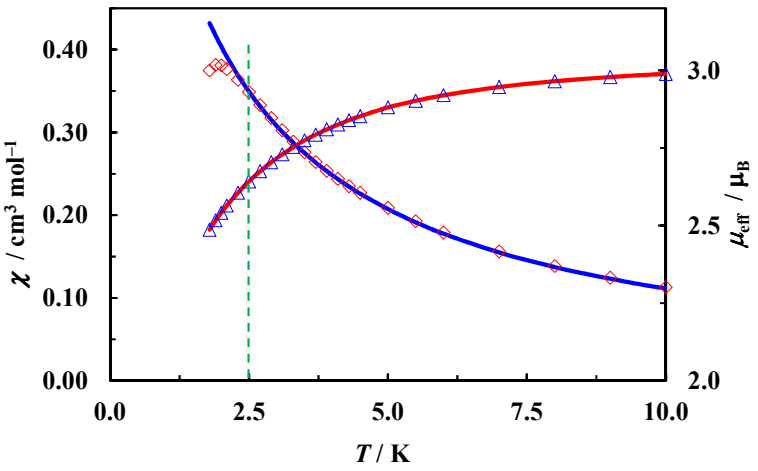

Fig. 7. Low temperature region of □ (◇) and □$_{eff}$ (Δ) versus *T* for **1**. The solid lines were calculated with the best fit parameters.

The moment is larger than the value of 2.83 □$_B$ expected for the spin-only value of an ion with *S* = 1 and *g* = 2.0, and lies within the range observed in other high-spin Ni(II) compounds.[64] The effective magnetic moment slowly decreases from 3.06 μ_B at 300 K to 3.02 μ_B at 20 K and then drops to 2.47 μ_B at 1.8 K. The decrease in the moment below 10 K could be caused by a zero-field splitting and/or by antiferromagnetic exchange interactions between the metal ions. The first three points of magnetic susceptibility are deflected toward the abscissa, creating the maximum in the vicinity of 1.9 K. Because it was not possible to simulate this maximum using the methods applied in this work, all the susceptibility calculations were carried out in the temperature range 2.5 - 300 K. Assuming that only the zfs is responsible for low-temperature effects, we have calculated magnetization of the isolated Ni(II) ion by the full matrix diagonalization of the Hamiltonian (1) . When using the HFEPR parameters (D = –5.745 cm^{-1}, E = –0.428 cm^{-1}, g_x = 2.162, g_y = 2.157, g_z = 2.190), a rather poor agreement between the calculated and experimental data was obtained (the dotted line in Fig. 6). While the low temperature susceptibility may be affected by the magnetic exchange interactions, the data in the medium and high temperature range depend mainly on the *g* factor. Much better results have been achieved when the *g*-factor was allowed to change. The fitting of the temperature dependence of susceptibility (Figs. 6 and 7) with D = –5.745 cm^{-1}, E = –0.428 cm^{-1} (HFEPR values), g_x = 2.139, g_y = 2.132, g_z = 2.166, and the temperature independent susceptibility *N*□ = 41·10^{-6} gave the agreement factor $R = \Sigma[(\chi T)_{exp} - (\chi T)_{calc}]^2 / \Sigma[(\chi T)_{exp}]^2$ = 2.4·10^{-5} (61 points, starting with 2.5 K). The *g* values are lower by 1.1% than the corresponding HFEPR values. Such

a phenomenon, when *g* determined from magnetic susceptibility slightly differs from EPR value, is not rare, see for example [31, 65] and sometimes can help in the determination of the effective molar mass of a sample at the time of the magnetic measurements.[31b] A possibility of partial loss of non-coordinated water from complex **1** indeed cannot be completely ruled out in our case. A discrepancy between the low temperature experimental and calculated data can be caused by magnetic exchange interactions, but their value is expected to be small. Each of the nickel(II) ions of **1** is connected to two neighbors by 4,4'-bpy bridges, creating a linear chain running parallel to the unit cell *c* axis with the metal-metal distance of 11.452 Å. 4,4'-bpy is used as a rigid spacer in the modular design of coordination networks.[66-69] It is known to be a weak transmitter of magnetic interactions, because of: (i) large length of the 4,4'-bpy bridge, (ii) unfavorable orbital overlap across the bridge, influenced by the torsion angle between the pyridine rings, (iii) the single C–C bond between the pyridine rings, which suppresses the conjugation of the two halved 4,4'-bpy molecules.[70] The importance of the first of these factors should not be overestimated, considering the recent report of measurable magnetic coupling at the Cu···Cu distance equal to 22 Å.[71] As can be noticed, the magnetic coupling is generally antiferromagnetic and very weak for 3*d* ions. The antiferromagnetic character is consistent with the McConnell spin-polarization mechanism, according to which the interaction alternates in sign if the bridging pathway between the metal centers increases or decreases by one atom (Table 3). [74, 78]

Table 3 Magnetic properties of compounds with the 4,4'-bpy bridges.

Compound	*J*	*g*	□	□	Ref.
	cm^{-1}		K	°	
$[Cu_2(ClO_4)_2(dien)_2(4,4'\text{-bpy})](ClO_4)_2$	–0.3	2.03	–0.4	0.00	72

$[Cu(NO_3)_2(2,2'\text{-bpy})(4,4'\text{-bpy})]_n \cdot 2nCH_3OH$	–0.53	2.01	–1.8	0.00	73
$[\{Mn(BMA)(SCN)_2\}_2]\cdot(\mu\text{-}4,4'\text{-bpy})$	–0.044	2.02	-	0.00	70
$[\{Mo^{I}(NO)Tp^{*}Cl\}_2(\mu\text{-}4,4'\text{-bpy})]$	–33	1.971	–33	26 (calc)	74, 75
$[\{Ni(BMA)(SCN)_2\}_2]\cdot(\mu\text{-}4,4'\text{-bpy})(DMSO)_2$	–0.32	2.20	-	0.00	70
$[Ni(Bu\text{-}dtp)_2(4,4'\text{-bpy})]_n$	-	-	–32	37.52	76
$[Ni(4,4'\text{-bpy})_{1.5}(H_2O)_2(BA)_2]\cdot H_2O$	15.76	2.05	-	0.00	77
$[Ni(4,4'\text{-bpy})(HMBA)(MBA)_2]_n$	7.32	2.01	-	6.20	77
$\{[Ni(L\text{-}Tyr)_2(\mu\text{-}4,4'\text{-bpy})]\cdot 4H_2O\}_n$	$\lvert zJ' \rvert < 0.05$	2.15	–1.1	12.66	This work

Two distinctive compounds in Table 3 are the nickel complexes with benzoic and *p*-methylbenzoic acids.[77] Their exchange integrals could raise some doubts: both were found without taking into account any zfs effects, which are clearly visible in the magnetic susceptibility graphs and should strongly affect the ferromagnetic ground state, moreover, the formula describing the susceptibility of a nickel dimer used in Ref. 77 refers to the case $S_1 = S_2 = 5/2$.

The other way of transferring the magnetic exchange can be provided by hydrogen bonds. The metal ions are linked by the long Ni–O11–C11–O12···H21A–N21–Ni bonds, forming a zig-zag chain extended parallel to the *b* axis, but a large Ni···Ni distance (8.556 Å) and unfavorable hydrogen bond parameters (D···A distance of 3.211 Å and the D···H–A bond angle equal to 121.4°) exclude any substantial magnetic coupling. Two different approaches were tried in fitting the data including the effect of magnetic coupling. In the first attempt a molecular field parameter zJ' was introduced in a form of $\chi = \chi_{zfs} / (1 - zJ'\chi_{zfs} / Ng_{av}^2\beta^2)$ but no

significant improvement of the fit was achieved. In the next step we have tried to adapt the experimental susceptibility data to the model of Papanicolaou and Spathis.[81] They have considered S = 1 Heisenberg chain with a strong easy-plane anisotropy and calculated the susceptibility up to second order perturbation term. Here, too, we were not able to obtain a meaningful value of the magnetic coupling parameter. In conclusion, magnetic interactions affect the low-temperature magnetic properties, but it is not possible to describe them using a single exchange integral. The analysis of the field dependent magnetization confirmed the weakness of magnetic interactions in **1**. The $M(B)$ dependence calculated for different external fields with the same parameters as the susceptibility is drawn in Fig. S4, and fits the experimental data excellently at 5.0 K and slightly worse at 2 K, which is not surprising, given the close proximity of the susceptibility maximum (Fig.S3).

The TGA plots indicate at least a three-stage decomposition process in nitrogen atmosphere (Fig. S6). The endotherms in the temperature range 50-110 ^{o}C, are assigned to the loss of two water molecules (O2 and O3) (Table 4).

Table 4 Summary of TG-DTA and DSC analyses data of (**1**).

Stage	$T^*_{deh,i}$ (°C)	T^*_{max} (°C)	ΔH° (J g^{-1})**	Evolved moiety formula	Weight loss (%)	Mass calc. (%)
1	53	95.86	130.34	0.5 H_2O	4.88	5.56
			80.37	1.5 H_2O		
2	228	293	190	$2H_2O$	29.35	29.69
				4,4′-bpy		
3	334	458	- 7 318	L-Tyr	23.22	25.05

*Experiments carried out under nitrogen atmosphere; **experiments carried out in presence of air as the furnace atmosphere

With the removing two water molecules the sample mass decrease by 4.88 % (calc. 5.56%). In the second stage, sample remains stable from 230 ^{o}C to 320 ^{o}C. The rapid decomposition results in a loss of 29.35 % mass and is evidence for the elimination of the next two water molecules (O1 and O4) together with 4,4'-bpy molecule. The anhydrous sample decompose between 330 ^{o}C and 500 ^{o}C with 23.22 % mass lost (calc. 25.05 %). The DSC curve displayed a strong exothermic overlapped peaks attributed to the oxidative decomposition of organic fragments. The final decomposition black product was a mixture of NiO as well as Ni_2O_3 (found 42.5 %, calc. 37.09 %)

DFT results. For the optimized structure of the [Ni(L-Tyr)$_2$(μ-4,4'-bpy)$_2$] complex, it was found that the ΔE for the 4,4'-bpy ligands is *ca.* -20 kcal mol^{-1}, while the $|\Delta E|$ for the L-tyrosine ligand was calculated to be about one order of magnitude higher (ΔE = -153 kcal mol^{-1}). When a crystal of **1** is dissolved in DMSO, 4,4'-bpy molecules can be replaced by water and/or DMSO molecules. The L1 and L2 ligands have different surrounding (Fig. 8).

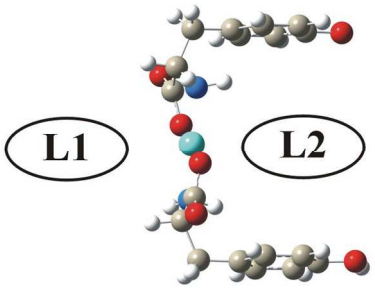

Fig. 8 Drawing of the [Ni(L-Tyr)$_2$L1L2] complex (where L1, L2 = 4,4'-bpy, H_2O, DMSO).

Since at each position (L1 and L2) one of three ligands (4,4'-bpy, H_2O, DMSO) can be located, nine different complexes are possible. For the complexes 1, 2 and 3 (where the L1 and L2 ligands are the same), the calculated ΔE for the L2 ligand is larger than that obtained for the L1 by 2.47, 3.89 and 2.28 kcal mol^{-1} for 4,4'-bpy, H_2O and DMSO, respectively (Table 5). In contrast to L1, the L2 ligand is located between two L-tyrosine rings (Fig. S7).

Table 5 DFT calculated interaction energies (ΔE) corrected for the BSSE between selected ligand and the rest of the complex in nine complexes considered.

no	L1	L2	ΔE(L1)	ΔE(L2)
1	4,4'-bpy	4,4'-bpy	-15.73 (4.75)[a]	-18.20 (6.41)
2	H_2O	H_2O	-12.14 (4.66)	-16.03 (5.03)
3	DMSO	DMSO	-19.01 (7.49)	-21.29 (7.78)
4	H_2O	DMSO	-10.02 (4.97)	-27.31 (7.76)
5	DMSO	H_2O	-23.61 (7.51)	-13.88 (5.43)
6	DMSO	4,4'-bpy	-19.44 (7.62)	-17.49 (6.26)
7	4,4'-bpy	DMSO	-15.08 (4.70)	-22.12 (7.92)
8	H_2O	4,4'-bpy	-9.25 (4.68)	-21.73 (6.32)
9	4,4'-bpy	H_2O	-20.10 (4.73)	-11.24 (6.10)

[a]in parenthesis there is value of BSSE

Probably, in the case of the more strongly bound ligand (L2), additional stabilizing interactions between L-tyr rings and L2 are responsible for this effect. Whereas, the interaction energies obtained for DMSO are in the range from - 19.01 (for L1 in **3**) to -27.31 kcal mol^{-1} (in **4**,

L1 = H_2O). In the case of the 4,4'-bpy ligand the calculated ΔE varies between -15.08 kcal mol^{-1} (in **7**, L2 = DMSO) and -21.73 kcal mol^{-1} (in **8**, with L1 = H_2O). The ΔE for H_2O are in the range between - 9.25 and - 16.03 kcal mol^{-1} in the complexes 8 and 2, respectively. Thus, it can be concluded that among the three ligands considered, DMSO is the most strongly bound, while the H_2O molecule is the most weakly bound one. The most likely mechanism of the ligands exchange reaction when **1** is dissolved in aqueous solution of DMSO, can be proposed. This proposed mechanism of the ligand exchange process can be described as a two-step process :

$[Ni(L\text{-}Tyr)_2(\mu\text{-}4,4'\text{-}bpy)_2] + DMSO \rightarrow [Ni(L\text{-}Tyr)_2(\mu\text{-}4,4'\text{-}bpy)DMSO] + 4,4'\text{-}bpy$ step 1

$[Ni(L\text{-}Tyr)_2(\mu\text{-}4,4'\text{-}bpy)DMSO] + DMSO \rightarrow [Ni(L\text{-}Tyr)_2DMSO_2] + 4,4'\text{-}bpy$ step 2

In the first step, the weakly bound 4,4'-bpy ligand (L1) is exchanged for a DMSO molecule (in **6**). It is worth mentioning that the DMSO presence in complex 6 causes a ΔE decrease for the 4,4'-bpy ligand. In the case of complex 1, that ΔE for the 4,4'-bpy ligand (L2) is - 18.20 kcal mol^{-1}, while in **6** it is - 17.49 kcal mol^{-1}. In the next step, the second 4,4'-bpy ligand (L2) is also exchanged for DMSO and finally the $[Ni(L\text{-}Tyr)_2(DMSO)_2]$ complex is formed.

The absorbance spectrum of complex **1** in DMSO exhibits three bands correlated with three *d-d* transition in O_h model with energies 9900 cm^{-1}, 16250 cm^{-1} and 27250 cm^{-1} arise from $^3A_{2g} \rightarrow {}^3T_{2g}(^3F)$, $^3A_{2g} \rightarrow {}^3T_{1g}(^3F)$, and $^3A_{2g} \rightarrow {}^3T_{2g}(^3P)$ transitions (Fig. S7). Those three *d-d* bands are unsplited. Bands assigned to the spin-forbidden $^3A_{2g} \rightarrow {}^1E_g$ as well as $^3A_{2g} \rightarrow {}^1A_{1g}(G) + {}^1T_{1g}(G)$ transitions are also visible at 13200 cm^{-1} and 21300 cm^{-1}. The transition energies gave the crystal field parameters: Dq = 994 cm^{-1} and B = 908 cm^{-1}, C = 3215 cm^{-1} (C/B = 3.56). The D_{4h} symmetry of Ni^{2+} ions found in solid **1** changes to O_h symmetry in DMSO solutions. This effect is caused by changing ligands in the coordination sphere. The structural analog {[Zn(L-Tyr)$_2$(μ-4,4'-

bpy)]·4H_2O}$_n$ [61] exhibits the very weak binding of the 4,4'-bpy molecule. The interaction energies (ΔE) between N1– and N2–coordinated 4,4'-bpy and the rest of the complex calculated from DFT equal *c.a.* -14 kcal mol^{-1}, while in the case of the chelating bonded L-tyrosinate anions the absolute values are much larger (ΔE is about -155 kcal mol^{-1}). The comparison of ^{1}H and ^{13}C NMR spectra of {[Zn(L-Tyr)$_2$(μ-4,4'-bpy)]·4H_2O}$_n$ and free 4,4'-bpy exhibits minor differences in chemical shifts for signals attributed to 4,4'-bpy H and C atoms. In the DMSO solution of {[Zn(L-Tyr)$_2$(μ-4,4'-bpy)]·4H_2O}$_n$, the 4,4'-bpy molecules exist as non-coordinated. Similar DFT results were obtained for **1**. This means that the mechanism of removing 4,4'-bpy molecule can also be applied to explain the nickel(II) behavior in DMSO. In this way, the octahedral Ni^{2+} ions environment can be supplemented by H_2O as well as DMSO molecules and both molecules can be coordinated via O atoms resulting in a pseudo octahedral environment.

4. CONCLUSIONS

In summary, rare nickel(II) L-tyrosinate 1D-coordination polymer, {[Ni(L-Tyr)$_2$(μ-4,4'-bpy)]·4H$_2$O}$_n$ (**1**) is reported. The tetragonality parameter T equals 0.945 and this distortion of octahedron is the largest among all other structures L-tyrosinato nickel(II) complexes. The absorbance electronic spectra indicated a change in the tetragonally distorted NiN$_2$N$_2$'O2 chromophore by removing of 4,4'-bpy molecules upon dissolution. The cracking of Ni1—N1 and Ni1—N2^{i} bonds results from relatively week atoms interactions, ΔE is *ca.* -20 kcal mol^{-1} for the 4,4'-bpy. The values of Hamiltonian parameters g_x = 2.162(3), g_y = 2.157(3), g_z = 2.190(5), D = -5.74(2) cm^{-1}, E = -0.429(7) stay in reasonable agreement with the corresponding values obtained from the magnetic susceptibility fitting (g_x = 2.162, g_y = 2.155, g_z = 2.189). In crystals, the weakness of magnetic interactions was found because of large length of the 4,4'-bpy bridge (Ni···Ni 11.452 Å) as well as the long Ni–O11–C11–O12^{ii}···H21A–N21–Ni bonds (Ni···Ni distance 8.556 Å).

ACKNOWLEDGMENTS. The work was financed by a statutory activity subsidy from the Polish Ministry of Science and Higher Education for the Faculty of Chemistry of Wrocław University of Technology. The HF EPR spectra were recorded at the NHMFL, which is funded by the NSF through the Cooperative Agreement DMR-1157490, the State of Florida, and the DOE. The generous computer time from the Wroclaw and Poznan Supercomputer and Networking Centers is acknowledged. Project supported by Wroclaw Centre of Biotechnology, program The Leading National Research Centre (KNOW) for years 2014-2018. The assistance of Dr Saeed Doroudiani in language correction is gratefully acknowledged.

REFERENCES

1 A. S. Gelbard, A. J. L. Cooper, Y. Asano, E. Nieves, S. Filc-Dericco and K. C. Rosenspire, *Appl. Radiat. Isot.*, 1990, **41**, 229-233.

2 R. K. Evans, Z. Xu, K. E. Bohannon, B. Wang, M. W. Bruner and D. B. J. Volkin, *Pharm.Sciences*, 2000, **89**, 76-87.

3 P. F. Fitzpatric, *J. Am. Chem. Soc.*, 1994, **116**, 1133-1134.

4 L. Elsellami, F. Vocanson, F. Dappozze, E. Puzenat, O. Paisse, A. Houas and C. Guillard, *Applied Catalysis A: General*, 2010, **380**, 142-148.

5 (a) S. Ishimitsu, S. Fujimoto and A. Ohara, *Chem. Pharm. Bull.*, 1990, **38**, 1417-1418. (b) Z. Maskos, J. D. Rush and W. H. Koppenol, *Archiv. Biochem. Biophys.*, 1992, **296**, 521-529.

6 A. Nakagawa, H. Minami, J. S. Kim, T. Koyanagi, T. Katayama, F. Sato and H. Kumagai, *Nat. Commun*., 2012, **3:819**, 1-8.

7 D. Juminaga, E. E. K. Baidoo, A. M. Redding-Johanson, T. S. Batth, H. Burd, A. Mukhopadhyay, Ch. J. Petzold and J. D. Keasling, *Appl. Environ. Microbiol.*, 2012, **78**, 89-98.

8 E. Jung, O. L. Zamir and R. A. Jensen, *Proc. Natal. Acad. Sci.*, 1986, **83**, 7231-7235.

9 M. Ikeda, *Appl. Microbiol. Biotechnol.*, 2006, **69**, 615- 626.

10 Y. Satoh, K. Tajima, M. Munekata, J. D. Keasling and T. S. Lee, *Metabolic Engin.*, 2012, **14**, 603-610.

11 G. Eisenhofer, I. J. Kopin and D. S. Goldstein, *Pharmacol. Rev.*, 2004, **56**, 331-349.

12 M. M. Ryan, C. Sy, S. Rudge, C. Ellaway, D. Ketteridge, L. G. Roddick, S. T. Iannaccone, A. J. Kornberg and K. N. North, *J. Child Neurol.*, 2008, **23**, 609-613.

13 F. J. van Spronsen, M. van Rijn, J. Bekhof, R. Koch and P. G. Smit, *Am. J. Clin. Nutr*., 2001, **73**, 153-157.

14 E. R. Braverman, *The Healing Nutrients Within Facts, Findings, and New Research on Amino Acids*, 3-rd Edition, 2003.

15 J. M. Azorin, P. Bovier, J. Widmer, R. Jeanningros and R. Tissot, *Biol. Psychiatry*, 1990, **27**, 723-734.

16 S. N. Young, *J. Psych. Neuroscience*, 2007, **32**, 80-82.

17 Ch. N. S. Santos and G. Stephanopulos, *Appl. Environ. Microbiol.*, 2008, **74**, 1190-1197.

18 A. Slonimski, M. Żmijewski and J. Pawelek, *Pigment Cell Melanoma Res.*, 2011, **25**, 14-27.

19 Z. Glick, S. Wu, J. Lupien, R. Reggio, G. Bray and D. Fisher, *Am. J. Physiol.*, 1985, **249**, 519-524.

20 D. L. Johannsen, J. E. Galgani, N. M. Johannsen, Z. Zhang, J. D. Covington and E. Ravussin, *PLoS ONE*, 2012, **7**, e40837.

21 J. R. Chalmers, G. T. Dickson, J. Elks and B. A. Hems, *J. Chem. Soc*., 1949, 3424-3433.

22 R. G. Elkin, W. R. Featherston and J. C. Rogler, *J. Nutr.*, 1980, **110**, 130-138.

23 X. Zhang, G. Wang, X. Liu, H. Wu and B. Fang, *Cryst. Grow. Design*., 2008, **8**, 1430-1434.

24 I. A. Khan, M. Bano and E. Kabir-ud-Din, *J. Disper. Science Technol*., 2010, **31**, 177-182.

25 G. Thirupathi, M. Venkatanarayana, P. K. Dubey, Y. Bharathi Kumari, *Organic Chem. International*, 2012, **2012**, 1-4.

26 (a) X. Huang, Ch. Y. Shen, J. Ch. Chen and Q. J. Li, *Biomaterials Science*, 2009, **20**, 935-955. (b) M. Spagnuolo and L. Liu, *Nanotechnology*, **2012**, 1-11. (c) P. N. Shah and Y. H. Yun, *J. Biomater. Appl*, 2013, **27**, 1017-1031.

27 H. J. Wester, M. Herz, W. Weber, P. Heiss, R. Senekowitsch-Schmidtke, M. Schwaiger and G. Stocklin, *J. Nucl Med.*, 1999, **40**, 205-212.

28 B. S. Moon, S. W. Kim, T. S. Lee, S. H. Ahn, K. Ch. Lee, G. An, S. D. Yang, D. Y. Chi, Ch. W. Choi, S. M. Lim and K. S. Chun, *Bull. Korean Chem. Soc*., 2005, **26**, 91-96.

29 R. Hamalainen, M. Ahlgren, U. Turpeinen and T. Raikas, *Cryst. Struct. Commun*., 1978, **7**, 379-384.

30 A. Wojciechowska, M. Daszkiewicz, Z. Staszak, A. Trusz-Zdybek, A. Bienko and A. Ozarowski, *Inorg. Chem.*, 2011, **50***,* 11532-11542.

31 A. Wojciechowska, A. Gagor, M. Duczmal, Z. Staszak and A. Ozarowski, *Inorg. Chem*., 2013, **52**, 4360-4371.

32 A. Wojciechowska, A. Kochel and M. Komorowska, *Polyhedron*, 2011, **30**, 2361-2367.

33 A. Wojciechowska, A. Gagor, R. Wysokiński and A. Trusz-Zdybek, *J. Inorg. Biochem.*, 2012, **117**, 93-102.

34 (a) D. U. Miodragovic, G. A. Bogdanovic, S. M. Milosavljevic, M. J. Malinar, M. B. Celap, A. Spasojevic-de Bire, S. Macura and N. Juranic, *Enantiomer*, 2001, **6**, 299-308. (b) O. Yamauchi, A. Odani, T. Kohzuma, H. Masuda, K. Toriumi and K. Sato, *Inorg. Chem.*, 1989, **28**, 4066-4068. (c) X. Solans, L. Ruiz-Ramirez, A. Martinez, L. Gasque and R. Moreno-Esparza, *Acta Cryst*., 1992, **C48**, 1785-1788. (d) F. Zhang, T. Yajima, H. Masuda, A. Odani and O. Yamauchi, *Inorg. Chem*., 1997, **36**, 5777-5784. (e) E. J. Gao, H. Y. Li and Q. T. Liu, *Acta Chim. Sinica*, 2005, **63**, 1225-1230. (f) G. Qin, L. Xue-Yi, L. Qing-Bin, L. Sheng-Rong, M. Xue-Dan and F. Xiao-Long, *Chin. J. Chem.*, 2007, **25**, 791-796. (g) O. Yamauchi, A. Odani and H. Masuda, *Inorg. Chim. Acta*, 1992, **198**, 749-761. (h) S. Q. Li and N. H. Hu, *Acta Crystallogr.*, 2011, **E67**, m884-m885.

35 (a) S. Q. Li and N. H. Hu, *Acta Crystallogr., Sect. E.*, 2012, **E68**, m633-m634. (b) B. Zhou, N. J. O. Silva, F. N. Shi, F. Palacio, L. Mafra and J. Rocha, *Eur. J. Inorg. Chem.*, 2012, **2012**, 5259-5268. (c) J. Weng, M. Hong, Q. Shi, R. Cao and A. S. C. Chan, *Eur. J. Inorg. Chem*., **2002**, 2553-2556.

36 F. Apfelbaum-Tibika and A. Bino, *Inorg. Chem*., 1984, **23**, 2902-2905.

37 W. Liu, Y. Song, Y. Li, Y. Zou, D. Dang, Ch. Ni and Q. Meng, *Chem Commun.*, **2004**, 2348-2349.

38 D. Q. Li, J. Zhou and X. Liu, *Acta Cryst*., 2007, **C63**, m371-m373.

39 T. Kiss and A. Gergely, *J. Chem. Soc. Dalton Trans.*, **1984**, 1951-1957.

40 A. S. Molchanov and S. F. Ledenkov, *Russ. J. Phys*. *Chem. A*, 2009*,* **28***,* 2028-2031.

41 P. Djurdjevic, R. Jelic, D. Dzajevic and M. Cvijoviv, *Met. Based Drugs*, 2006, **8**, 235-248.

42 S. Majid, M. E. Rhazi, A. Amine and Ch. Brett, *Analytica Chimica Acta*, 2002, **464**, 123-133.

43 S. Kumar and O. D. Gupta, *Oriental J. Chem.*, 2010, **26**, 697-699.

44 (a) H. Xu and L. Chen, *Spectrochimica Acta A*, 2003, **59**, 657-662. (b) I. J. Bruno, J. C. Cole, P. R. Edgington, M. Kessler, C. F. Macrae, P. McCabe, S. Hem, J. Pearson and R. Taylor, *Acta Cryst.*, 2002, **B58**, 389. CSD version 5.31.

45 Y. Pei and L. Wang, *Acta Crystallogr*., *Sect. E*, 2006, **62**, m1668-m1670.

46 CrystAlis CCD and CrystAlis Red program, Ver. 171.31.8 Oxford Diffraction Poland, Wrocław, Poland 2006.

47 G. M. Sheldrick, SHELXS97, SHELXL97, Programs for Crystal Structure Solution and Refinement, University of Göttingen, Göttingen, Germany, 1997.

48 K. Brandenburg and H. Putz, Diamond, Ver. 3.0 Crystal and Molecular Structure Visualization, University of Bonn, Germany, 2006.

49 (a) A. D. Becke, *J. Chem Phys*, 1996, **104**, 1040-1046. (b) A. D. Becke, *J. Chem Phys*, 1993, **98**, 5648-5652.

50 C. Lee, W. Yang and R. G. Parr, *Phys. Rev. B*, 1988, **37**, 785-789.

51 T. H. Dunning Jr. and P. J. Hay, in Modern Theoretical Chemistry, Ed. H. F. Schaefer III, Vol. 3 (Plenum, New York, 1976) 1-28.

52 P. J. Hay and W. R. Wadt, *J. Chem. Phys.*, 1985, **82**, 299-310.

53 S. F. Boys and F. Bernardi, *Mol*. *Phys*., 1970, **19**, 553-566 .

54 M. J. Frisch, G. W. Trucks, H. B. Schlegel, G. E. Scuseria, M. A. Robb, J. R. Cheeseman, G. Scalmani, V. Barone, B. Mennucci, G. A. Petersson, H. Nakatsuji, M. Caricato, X. Li, H. P. Hratchian, A. F. Izmaylov, J. Bloino, G. Zheng, J. L. Sonnenberg, M. Hada, M. Ehara, K. Toyota, R. Fukuda, J. Hasegawa, M. Ishida, T. Nakajima, Y. Honda, O. Kitao, H. Nakai, T. Vreven, J. A. Montgomery Jr, J. E. Peralta, F. Ogliaro, M. Bearpark, J. J. Heyd, E. Brothers, K. N. Kudin, V. N. Staroverov, R. Kobayashi, J. Normand, K. Raghavachari, A. Rendell, J. C. Burant, S. S. Iyengar, J. Tomasi, M. Cossi, N. Rega, J. M. Millam, M. Klene, J. E. Knox, J. B. Cross, V. Bakken, C. Adamo, J. Jaramillo, R. Gomperts, R. E. Stratmann, O. Yazyev, A. J. Austin, R. Cammi, C. Pomelli, J. W. Ochterski, R. L. Martin, K. Morokuma, V. G. Zakrzewski, G. A. Voth, P. Salvador, J. J. Dannenberg, S. Dapprich, A. D. Daniels, O. Farkas, J. B. Foresman, J. V. Ortiz, J. Cioslowski, D. J. Fox, Gaussian, Inc., Wallingford CT, 2009.

55 G. Bierman and H. Ziegler, *Anal. Chem.*, 1986, **58**, 536-539.

56 (a) J. Myrczek, *Spectr. Lett.*, 1990, **23**, 1027-1039. (b) A. Wojciechowska, W. Bronowska, A. Pietraszko, Z. Staszak and M. Cieślak-Golonka, *J. Mol. Struct.*, 2002, **608**, 151-160.

57 A. K. Hassan, L. A. Pardi, J. Krzystek, A. Sienkiewicz, P. Goy, M. Rohrer and L. C. Brunel, *Magn. Reson*., 2000, **142**, 300-312.

58 X. Feng, J. G. Wang, Ch. Z. Xie and N. Z. Ma, *Anorg. Allg. Chem.*, 2007, **633**, 2085-2088.

59 B. Murphy, M. Aljabri, A. M. Ahmed, G. Murphy, B. J. Hathaway, M. E. Light, T. Geilbrich and M. B. Hursthouse, *Dalton Trans.*, **2006**, 357-367.

60 (a) R. W. Seidel, R. Goddard, B. Zibrowius and I. M. Oppel, *Polymers*, 2011, **3**, 1458-1474. (b) J. T. Culp, A. L. Goodman, D. Chirdon, S. G. Sankar and Ch. Matranga, *J. Phys. Chem. C*, 2010, **114**, 2184-2191. (c) D. V. Soldanov, I. L. Moudrakovski, C. I. Ratcliffe, R. Dutrisac and J. A. Ripmeester, *Chem. Mater.*, 2003, **15**, 4810-4818.

61 A. Wojciechowska, J. Janczak, W. Zierkiewicz, A. Dylong and E. Matczak-Jon, *Polyhedron*, 2015, **85**, 665-674.

62 (a) A. Ozarowski, *Inorg. Chem*., 2008, **47**, 9760-9762. (b) A. Ozarowski, I. B. Szymanska, T. Muziol and J. Jezierska, *J. Am. Chem. Soc*., 2009, **131**, 10279-10292.

63 R. Boca, *Coord Chem. Rev.*, 2004, **248**, 757-815.

64 B. N. Figgis and M. A. Hitchman, *Ligand Field Theory and Its Applications*, Willey, New York 2000.

65 D. Maganas, J. Krzystek, E. Ferentinos, A. M. Whyte, N. Robertson, V. Psycharis, A. Terzis, F. Neese and P. Kyritsis, *Inorg. Chem*., 2012, **51**, 7218-7231.

66 L. Brammer, *Chem. Soc. Rev.*, 2004, **33**, 476-489.

67 K. Biradha, M. Sarkar and L. Rajput, *Chem. Commun.*, 2006, 4169-4179.

68 R. J. Kuppler, D. J. Timmons, Q. R. Fang, J. R. Li, T. A. Makal, M. D. Young, D. Yuan, D. Zhao, W. Zhuang and H. C. Zhou, *Coord. Chem. Rev*., 2009, **253**, 3042-3066.

69 A. Noor, E. S. Tamne, B. Oelkers, T. Bauer, S. Demeshko, F. Meyer, F. W. Heinemann and R. Kempe, *Inorg. Chem.*, 2014, **53**, 12283-12288.

70 Y. Z. Liu, Q. J. Su, X. Qiao, C. Z. Xie, Y. Ouyang, J. Y. Xu, D. Z. Liao and S. P. Yan, *Z. Anorg. Allg. Chem.*, 2010, **636**, 600-611.

71 M. Castellano, F. R. Fortea-Pérez, A. Bentama, S. E. Stiriba, M. Julve, F. Lloret, G. De Munno, D. Armentano, Y. Li, R. Ruiz-García and J. Cano, *Inorg. Chem.*, 2013, **52**, 7645-7657.

72 M. Julve, M. Verdaguer, J. Faus, F. Tinti, J. Mortal, A. Monge and E. Gutierrez-Puebla, *Inorg. Chem.*, 1987, **26**, 3520-3527.

73 H. W. Park, S. M. Sung, K. S. Min and M. P. Suh, *Eur. J. Inorg. Chem*., 2001, **2001**, 2857-2863.

74 A. M. W. Cargill-Thompson, D. Gatteschi, J. A. McCleverty, J. A. Navas, E. Rentschler and M. D. Ward, *Inorg. Chem.*, 1996, **35**, 2701-2703.

75 S. L. W. McWhinnie, C. J. Jones, J. A. McCleverty, D. Collison and F. E. Mabbs, *J. Chem. Soc., Chem. Commun.*, 1990, 940-942.

76 R. G. Xiong, Z. Yu, J. L. Zuo and X. Z. You, *Spectrosc. Lett.*, 1997, **30**, 403-413.

77 X. K. Yu, X. S. Zhai, Y. Q. Zheng and H. L. Zhu, *Z. Naturforsch.*, 2014, **69b**, 62-70.

78 H. M. McConnell, *J. Chem. Phys.*, 1963, **39**, 1910-1910.

79 N. Papanicolaou and P. Spathis, *Phys. Rev.*, 1995, **B52**, 16001-16011.